This article has been accepted for publication in a future proceedings of this conference, but has not been fully edited. Content may change prior to final publication.
Citation information: DOI: 10.1109/UPEC65436.2025.11279944, 2025 60th International Universities Power Engineering Conference (UPEC)

# System Sizing of Hybrid Renewable Systems Under Inverter and Contracted Grid Power Constraints with Flexible Load Integration

Abdelaziz Abualshawareb
*Department of Mechanical and Aerospace Engineering*
*Brunel University of London*
Uxbridge, United Kingdom
Abdelaziz.Abualshawareb2@brunel.ac.uk

Ioana Pisica
*Department of Electronic and Electrical Engineering*
*Brunel University of London*
Uxbridge, United Kingdom
Ioana.pisica@brunel.ac.uk

Carola König
*Department of Mechanical and Aerospace Engineering*
*Brunel University of London*
Uxbridge, United Kingdom
Carola.koenig@brunel.ac.uk

***Abstract*— Island microgrids face significant challenges, including seasonal load variations, weak interconnections, and high demand charges leading to oversized energy systems. This paper introduces a novel bi-level optimization approach, combining a genetic algorithm for capacity sizing and a rolling-horizon mixed-integer linear programming controller for daily dispatch scheduling. The method simultaneously optimizes photovoltaic arrays, battery storage, hydrogen tanks, inverter ratings, and contracted grid-import limits to minimize the net present cost. The approach was applied to a municipal energy community in Formentera, Spain, with an annual demand of approximately 203 megawatt-hours. Compared to the baseline scenario (661,677 euros), the proposed framework reduced the net present cost to 612,945 euros without load flexibility. Introducing load flexibility further decreased costs: 606,879 euros at 6 percent and 599,134 euros at 8 percent flexibility. Increased flexibility resulted in modest reductions in photovoltaic capacity from 155 to 150 kilowatt-peak, inverter size from 77 to 72 kilowatts, and contracted grid-import limits from 41 to 37 kilowatts. The findings underscore the significant economic and operational advantages of integrating demand-side flexibility into the co-optimization of component sizing, enhancing both the resilience and autonomy of islanded hybrid renewable energy systems.**

***Keywords— energy management system, microgrid, hydrogen, renewable energy, modelling.***

## I. INTRODUCTION

Island communities like Formentera face critical energy challenges due to geographic isolation, seasonal demand variability, and reliance on imported fossil fuels, often resulting in high generation costs and stressed infrastructure. Across the EU, over 16 million residents on 2,200 islands [1] encounter such conditions, exacerbated by ageing grids and limited renewable integration [1], [2]. Transitioning to decentralised, resilient systems is essential.

Hybrid renewable energy systems (HRES), combining PV, battery storage, and hydrogen, offer a promising path, with architectures ranging from DC and AC microgrids to hybrid AC/DC configurations that improve conversion efficiency and flexibility [3]. However, existing studies predominantly optimise component sizing using heuristics, often overlooking operational constraints such as inverter sizing, grid exchange limits, or demand-side flexibility [4], [5].

While some works enhance dispatch modelling, they are often limited to off-grid systems [6] or treat grid contracts and inverter capacity as fixed parameters [7]. More advanced studies integrate cost and emissions objectives or use predictive control [8], [9], but still neglect joint optimisation of inverter and grid contract capacities.

This paper proposes a nested optimisation framework coupling a Genetic Algorithm (GA) based system design with a rolling-horizon Mixed-Integer Linear Programming (MILP) dispatcher. It optimises inverter sizing, grid contracts, and storage operation under real-world tariff structures, incorporating demand flexibility and AC/DC hybrid flows. Applied to Formentera, the model addresses key operational and contractual constraints, offering a scalable approach for resilient island energy transitions.

## II. METHODOLOGY

The proposed framework introduces a bi-level optimisation strategy that integrates a GA with a rolling-horizon MILP model to optimise hybrid energy systems over a one-year horizon. The upper loop, responsible for long-term capacity sizing, uses a GA to minimise the system's Net Present Cost (NPC). It begins with the definition of demand profiles, technical constraints, and tariff structures, and then evolves system configurations through selection, crossover, and mutation operations. For each candidate solution, the lower loop performs short-term operational dispatch using a MILP controller.

Unlike traditional approaches that solve the MILP over all 8,760 hours of the year in a single batch, the proposed model decomposes the timeline into rolling 24-hour windows. Within each window, only the first 12 hours are committed to the final schedule, while the remainder is discarded and recalculated as the horizon advances by 12 hours. This structure emulates a Model Predictive Control (MPC) strategy, allowing for dynamic adjustment of load shifting and peak shaving decisions under time-of-use (ToU) pricing constraints. The MILP is responsible for determining hourly energy flows while respecting grid contract limits, inverter constraints, and component operating characteristics.

The result of each MILP execution is an hourly control strategy and associated operational cost. These are accumulated to construct an annual profile, which is then used in the GA's cash flow analysis, including capital investment, replacement scheduling, and end-of-life recovery, to compute the NPC. Once evaluated, the GA iterates to produce a new generation of candidate solutions. This nested structure ensures that each configuration is evaluated both economically and operationally, leading to optimal system sizing, cash flow dynamics, and dispatch strategy tailored for islanded or weak-grid contexts.

### A. GA-Upper Loop for Capacity Sizing

GA executes a global search over system design variables to identify the optimal combination of component sizes that minimise the system's NPC. Acting as the upper layer in the optimisation hierarchy, the GA iteratively evolves candidate solutions using selection, crossover, and mutation based on economic performance. The design vector for each individual is defined as:

$$X = \left[P_{PV}, N_{bt}, P_{inv}, P_{gr}, P_{fc}, P_{el}, S_{\mathrm{H}}\right] \tag{1}$$

In this vector, $P_{\mathrm{PV}}$ represents the installed photovoltaic capacity (kW), $N_{\mathrm{bt}}$ is the number of battery modules (each rated at 4.8 kWh ), $P_{\mathrm{inv}}$ is the inverter capacity (kW), and $P_{\mathrm{gr}}$ is the maximum allowable grid exchange capacity (kW). The terms $P_{\mathrm{fc}}$ and $P_{\mathrm{el}}$ denote the rated power of the fuel cell and electrolyser, respectively (in kW), and $S_{\mathrm{H}}$ is the hydrogen storage capacity (kg). The GA evaluates each candidate system configuration based on its NPC, which aggregates capital investment, operational costs, component replacements, and terminal salvage value across the system's lifetime. This fitness objective is formulated as:

$$\mathrm{minNPC} = \sum_{x \in \{\mathrm{k,\,t}\}} (C_x + O_x + R_x - S_x) \tag{2}$$

Where, $C_x, O_x, R_x,$ and $S_x$ represent the capital investment, operational expenditure, component replacement cost, and salvage value, respectively, for each component k during year $t$. These cost terms are inherently discounted using a yearly factor derived from the real interest rate. As part of the GA layer, photovoltaic (PV) output is pre-estimated using irradiance and temperature models and passed to the MILP layer for hourly dispatch optimization. The PV output is computed as:

$$p_{\mathrm{pv}}(t) = P_{PV} D_f \left(\frac{G_T\,(t)}{G_{T,STC}}\right)\left[1 + \alpha_p\left(T_c\,(t) - Tc_{,STC}\right)\right] \tag{3}$$

Where $P_{PV}$ is the rated power, $D_f$ is the derating factor, $G_T$ is the actual irradiance at time step t, $G_{T,STC}$ is the standard test condition irradiance, $\alpha_p$ is the temperature coefficient, $T_c$ is the cell temperature, and $Tc_{,STC}$ is the cell temperature at standard test conditions. The aggregated NPC functions as the GA's fitness metric, steering the optimisation process toward economically optimal system configurations. To discourage system configurations that result in persistent energy surplus or deficits, a conditional penalty term is introduced. This penalty is only applied when the total annual excess or unmet energy surpasses a defined threshold:

$$\psi = \begin{cases} \psi_{ex/un}, & \text{if } \sum_{t \in T} E_{ex/un}(t) > \epsilon \\ 0, & \text{otherwise} \end{cases} \tag{4}$$

Here, $\psi$ is the total penalty added to the objective function, $E_{ex/un}(t)$ represents either excess or unmet energy at hour $t$, and $\epsilon$ is a fixed energy threshold (e.g., 100 kWh). The constant $\psi_{ex/un}$ denotes the penalty magnitude in euros. This formulation ensures that system designs exhibiting poor energy balancing behaviour are penalised, guiding GA toward more resilient and well-balanced solutions.

### B. MILP- Local Loop for Rolling-Horizon Dispatch with Load Flexibility

The local layer of the proposed optimization framework utilizes a MILP model to minimize operational costs. The simulation horizon is divided into overlapping 24-hour windows, where only the initial 12 hours of each solution are fixed before the window advances by 12 hours. If a given window is indexed by $w$, its set of hourly time steps is denoted by:

$$\mathcal{T} \in \{0,1,\ldots,23\} \tag{5}$$

The objective of the MILP is to determine optimal dispatch decisions that minimise total grid-related expenditures over the year. This includes electricity purchases from the grid, revenue from energy exports, and penalties associated with unmet demand or curtailed excess energy. The objective function is presented as:

$$\min \sum_{t \in \mathcal{T}} \left[\pi_{\mathrm{buy}}\,(t) \cdot p_{\mathrm{in}}\,(t) - \pi_{\mathrm{sell}}\,(t) \cdot p_{\mathrm{out}}\,(t) + \lambda_{\mathrm{un}} \cdot e_{\mathrm{un}}\,(t) + \lambda_{\mathrm{ex}} \cdot e_{\mathrm{ex}}\,(t)\right] \tag{6}$$

Where $\pi_{\mathrm{buy}}\,(t)$ and $\pi_{\mathrm{sell}}\,(t)$ represent the electricity purchase and feed-in tariff rates in €/kWh at hour $t$, while $p_{\mathrm{in}}\,(t)$ and $p_{\mathrm{out}}\,(t)$ denote imported and exported power. The variables $e_{\mathrm{un}}\,(t)$ and $e_{\mathrm{ex}}\,(t)$ capture unmet load and curtailed renewable generation, respectively. Penalty values $\lambda_{\mathrm{un}}$ and $\lambda_{\mathrm{ex}}$ are scaled by a factor of 10:1 to reflect the prioritisation of load satisfaction over curtailment. These values align with typical practices found in MILP-based energy system literature [14].

The energy balance constraints ensure that, at each time step $t$, the total energy generated and exchanged within the system equals the energy consumed, while accounting for unmet demand and excess renewable output. These equations distinguish between DC and AC subsystems connected via an inverter, ensuring accurate tracking of internal flows and conversion losses. The DC-side energy balance is given by:

$$p_{\mathrm{pv,ac}}(t) + p_{\mathrm{pv,dc}}(t) + p_{\mathrm{bat,dis}}(t) + p_{\mathrm{fc}}(t) - p_{\mathrm{bat,cha}}(t) - \gamma_{\mathrm{inv}} \cdot p_{\mathrm{inv}}(t) - e_{\mathrm{ex}}(t) = 0\,, \qquad \forall t \in \mathcal{T} \tag{7}$$

The AC-side balance is formulated as:

$$p_{\mathrm{inv}}\,(t) + p_{\mathrm{in}}\,(t) - p_{\mathrm{out}}\,(t) - (p_{\mathrm{load}}\,(t) + (p_{\mathrm{flex}}\,(t)) - p_{\mathrm{el}}(t) + e_{\mathrm{un}}(t) = 0, \qquad \forall t \in \mathcal{T} \tag{8}$$

Where $p_{\mathrm{pv,ac}}(t)$ and $p_{\mathrm{pv,dc}}(t)$ represent the AC- and DC-side allocations of PV power, respectively. $p_{\mathrm{bat,\,dis}}\,(t)$ and $p_{\mathrm{bat,cha}}\,(t)$ are the battery discharge and charge powers, $p_{\mathrm{fc}}\,(t)$ is the fuel cell output, and $p_{\mathrm{el}}\,(t)$ is the electrolyser input. $p_{\mathrm{inv}}\,(t)$ is the inverter's output, scaled by the loss factor $\gamma_{\mathrm{inv}} = 1 + \left(1 - \eta_{\mathrm{inv}}\right)$, where $\eta_{\mathrm{inv}}$ is the nominal inverter efficiency (0.95). The terms $e_{\mathrm{ex}}(t)$ and $e_{\mathrm{un}}(t)$ quantify the curtailed renewable energy and unmet load, respectively. Grid interactions are captured by $p_{\mathrm{in}}\,(t)$ and $p_{\mathrm{out}}\,(t)$, representing energy purchased from and sold to the grid. $p_{\mathrm{load}}\,(t)$ and $p_{\mathrm{flex}}\,(t)$ correspond to the fixed and flexible components of AC demand, respectively. To ensure realistic operation, the

energy system is constrained such that it cannot simultaneously import and export power from the grid. This exclusivity is modelled using a binary variable $x_{\text{grid}}(t)$, which acts as a directional switch. The power flow from or to the grid at each time step $t \in \mathcal{T}$ is limited by the maximum contracted grid capacity $P_{\text{grid}}^{\max}$, as defined by:

$$p_{\text{in}}(t) \le P_{\text{grid}}^{\max} \cdot x_{\text{grid}}(t), \forall t \in \mathcal{T} \quad (9)$$

$$p_{\text{out}}(t) \le P_{\text{grid}}^{\max} \cdot \left(1 - x_{\text{grid}}(t)\right), \forall t \in \mathcal{T} \quad (10)$$

Similarly, to reflect battery operating constraints, charging and discharging actions are also modelled as mutually exclusive using the binary variable $x_{\text{bat}}(t)$. These are constrained by the respective charge and discharge power limits $P_{\text{bat}}^{-}$ and $P_{\text{bat}}^{+}$, leading to:

$$p_{\text{bat,cha}}(t) \le P_{\text{bat}}^{-} \cdot \left(1 - x_{\text{bat}}(t)\right), \forall t \in \mathcal{T} \quad (11)$$

$$p_{\text{bat,dis}}(t) \le P_{\text{bat}}^{+} \cdot x_{\text{bat}}(t), \forall t \in \mathcal{T} \quad (12)$$

These constraints ensure that the system adheres to physical limitations, allowing only one mode of operation (buy/sell or charge/discharge) per component at any given time step. To enforce mutually exclusive operation of the hydrogen subsystems, the model introduces a binary variable $x_{\text{hyd}}(t)$, which dictates whether the fuel cell or the electrolyser is active at any given time step $t \in \mathcal{T}$. Their respective operating limits are defined by their rated capacities $P_{\text{el}}$ for the electrolyser and $P_{\text{fc}}$ for the fuel cell. The operational constraints are given by:

$$p_{\text{el}}(t) \le P_{\text{el}} \cdot \left(1 - x_{\text{hyd}}(t)\right), \forall t \in \mathcal{T} \quad (13)$$

$$p_{\text{fc}}(t) \le P_{\text{fc}} \cdot x_{\text{hyd}}(t), \forall t \in \mathcal{T} \quad (14)$$

To ensure operational feasibility, the inverter's instantaneous output $p_{\text{inv}}(t)$ is constrained by its rated capacity $P_{\text{inv}}^{\max}$. This condition guarantees that the combined DC-side power converted to AC-whether originating from the battery, fuel cell, or PV subsystem-does not exceed the inverter's technical limit at any time step. This is represented as:

$$p_{\text{inv}}(t) \le P_{\text{inv}}^{\max}, \forall t \in \mathcal{T} \quad (15)$$

Finally, to ensure that all renewable energy generated at each time step is accurately partitioned, the model tracks the division of total PV output $p_{\text{pv}}(t)$ into AC-side consumption and DC-side availability:

$$p_{\text{pv,ac}}(t) + p_{\text{pv,dc}}(t) = p_{\text{pv}}(t), \forall t \in \mathcal{T} \quad (16)$$

After enforcing the inverter capacity constraint, any residual renewable energy on the DC side-denoted by $p_{\text{pv,dc}}(t)$ is either directed to charge the battery or, if unused, is recorded as curtailed excess energy $e_{\text{ex}}(t)$. This flow is captured by the following balance:

$$p_{\text{pv,dc}}(t) = p_{\text{bat,cha}}(t) + e_{\text{ex}}(t), \forall t \in \mathcal{T} \quad (17)$$

To prevent the battery from discharging when excess PV energy remains available at the DC bus (i.e., charging should take precedence), a conditional logic is applied using a binary variable $x_{\text{pv}}(t)$. This binary flag triggers battery charging when excess is present. The associated constraints are linearised via the big-M method as follows:

$$p_{\text{pv,dc}}(t) \le M \cdot x_{\text{pv}}(t) + \epsilon, \forall t \in \mathcal{T} \quad (18)$$

$$p_{\text{pv,dc}}(t) \ge \epsilon \cdot x_{\text{pv}}(t), \forall t \in \mathcal{T} \quad (19)$$

$$p_{\text{bat,dis}}(t) \le \left(1 - x_{\text{pv}}(t)\right) \cdot P_{\text{bat}}^{\max}, \forall t \in \mathcal{T} \quad (20)$$

Where $M$ is a large constant and $\epsilon$ is a small positive scalar used for numerical stability. The variable $x_{\text{pv}}(t)$ ensures that the battery is only discharged when no DC-side PV energy remains. The energy storage system's dynamics are captured by tracking the state of charge $\text{SoC}_{\text{bat}}(t)$ of the battery and the level of hydrogen (LoH) in the storage tank at each time step. The battery SoC is updated recursively using the following equation:

$$\text{SoC}_{\text{bat}}(t) = \begin{cases} \text{SoC}_{\text{init}}^{(w)}, & t = 0 \\ \text{SoC}_{\text{bat}}(t-1) + \dfrac{\eta_{\text{bat}}^{-} p_{\text{bat,cha}}(t)}{\eta_{\text{bat}} B_{\text{cap}}} - \dfrac{p_{\text{bat,das}}(t)}{\eta_{\text{bat}}^{+} n_{\text{bat}} B_{\text{cap}}}, & t > 0 \end{cases} \quad (21)$$

Where $\eta_{\text{bat}}^{-}$ and $\eta_{\text{bat}}^{+}$ are the charging and discharging efficiencies of the battery, $B_{\text{cap}}$ is the total energy capacity in kWh, and $n_{\text{bat}}$ is the number of battery units. The initial SoC at each rolling window $w$ is denoted $\text{SoC}_{\text{init}}^{(w)}$, carried over from the end of the prior window midpoint. Similarly, the hydrogen tank's level is computed using:

$$\text{LoH}(t) = \begin{cases} \text{LoH}_{\text{init}}^{(w)}, & t = 0 \\ \text{LoH}(t-1) + \dfrac{\eta_{\text{el}}}{P_{\text{HT}} H_{\text{LHV}}} p_{\text{el}}(t) - \dfrac{p_{\text{cc}}(t)}{\eta_{\text{tc}}^{+} P_{\text{HT}} H_{\text{LHV}}}, & t > 0 \end{cases} \quad (22)$$

Where $\eta_{\text{el}}$ and $\eta_{\text{fc}}^{+}$ are the electrolyser and fuel cell efficiencies, $P_{\text{HT}}$ is the hydrogen tank pressure in bar, and $H_{\text{LHV}}$ is the lower heating value of hydrogen (kWh/kg). The initial hydrogen level $\text{LoH}_{\text{init}}^{(w)}$ is carried from the midpoint of the prior window's committed segment. To incorporate demand-side flexibility, a binary decision variable is introduced to manage a shiftable load. At each hour $t$, the flexible load $p_{\text{flex}}(t)$ is either fully activated or deactivated based on the variable $x_{\text{flex}}(t)$, where:

$$p_{\text{flex}}(t) = P_{\text{flex}}^{\text{rated}} \cdot x_{\text{flex}}(t), \forall t \in \mathcal{T} \quad (23)$$

Here, $P_{\text{flex}}^{\text{rated}}$ is the fixed rated power (kW) of the flexible load, and $x_{\text{flex}}(t) \in \{0,1\}$ indicates whether the load is active at time $t$. The model enforces a daily run-time constraint to ensure the flexible load operates for a fixed number of hours $H_{\text{flex}}^{\text{daily}}$ within each day $d$. If $\mathcal{T}_d$ is the set of hours in day $d$, then:

$$\sum_{k \in \mathcal{T}_d} x_{\text{flex}}(k) = H_{\text{flex}}^{\text{daily}}, \forall d \quad (24)$$

Since the rolling horizon window can span across multiple days, the model tracks prior activations using a carryover term $\phi_d^{(w-1)}$, representing the number of flexible hours already used for day $d$ in previous windows. The total must still meet the daily target:

$$\sum_{k\in\mathcal{T}_d} x_{\text{flex}}(k) + \phi_d^{(w-1)} = H_{\text{flex}}^{\text{daily}}, \forall d \tag{25}$$

This formulation ensures consistent and fair allocation of flexible load hours over the course of each day, regardless of how rolling windows intersect with calendar days.

## III. Model Setup

### A. Case Study: Formentera Energy Community

Formentera, the southernmost of Spain's Balearic Islands, is electrically connected to the neighbouring island of Ibiza via two submarine cables, one rated at 132 kV and another at 30 kV. Despite hosting a local 2 MW solar PV installation, the island's electricity supply is predominantly reliant on mainland imports. Seasonal variations in demand are pronounced, ranging from approximately 7 MW during winter to peaks of 18 MW in the summer months.

The case study focuses on a municipal energy community located west of Sant Francesc Xavier. The cluster comprises seven public-sector buildings, including a town hall, schools, emergency services, and utility facilities. These buildings represent diverse load profiles, making them ideal for evaluating flexible and decentralized energy solutions.

An annual hourly load profile based on data collected during the VPP4Islands project [10] with a total annual demand of 202,905 kWh and a peak load of 67.91 kW. To simulate PV performance, the model incorporates solar irradiance and ambient temperature data retrieved from NASA's POWER database [11], aligned with Formentera's geographical coordinates.

### B. Technical and Economic Inputs

The techno-economic model draws on a combination of manufacturer specifications, literature, and pilot-specific data. Table I summarizes key component-level assumptions.

TABLE I. Techno-Economic Parameters

| Component | Cost | Maintenance | Efficiency | Lifetime |
|---|---|---|---|---|
| PV Panel | €1600/kW | €10/kW·yr | 20% | 25 years |
| Battery | €230/kWh | €10/kWh·yr | 95% | 8000 cycles |
| Inverter | €300/kW | €10/kW·yr | 96% | 20 years |
| Fuel Cell | €1200/kW | €0.02/kWh | 43% | 15,000 hours |
| Electrolyser | €1200/kW | €0.05/kWh | 63% | 35,000 hours |
| $H_2$ Tank | €500/kg | €10/kg·yr | – | 15 years |

In addition to technical parameters, the economic assessment incorporated key financial assumptions: an 8% nominal discount rate, 2% inflation, and an electricity price escalation rate of 3% to reflect long-term market evolution. The electricity price, inclusive of tax, was taken as 5.11%, while the standard value-added tax (VAT) applied was 21%, consistent with Spanish regulatory conditions. These assumptions were selected based on prevailing community energy investment benchmarks and historical trends.

### C. Grid Tariff Structure

The grid tariff applied in this study follows Endesa's commercial six-period time-of-use pricing, with base energy rates ranging from 0.376011 €/kWh in period 1 down to 0.277946 €/kWh in period 6, base power rates from 0.038308 €/kW to 0.005483 €/kW across the same periods, and a fixed export tariff of 0.051000 €/kWh. This data was obtained through the VPP4Islands pilot and includes dynamic pricing for both energy consumption and contracted capacity, with validation from the local utility operator.

The financial model incorporates four distinct billing components: the contracted power charge $F_{\text{cp}}$, energy consumption charge $E_{\text{cc}}$, peak demand penalty $F_{\text{ep,}}$, and revenue from exported electricity $S_{\text{bc}}$. These are computed using the following expressions:

$$F_{\text{cp}} = \sum_{p=1}^{P} \rho_p \cdot R_p \cdot D_{\text{month}} \tag{26}$$

$$E_{\text{cc}} = \sum_{t\in\mathcal{T}} p_{\text{in}}(t) \cdot \pi_{\text{buy}}(t) \tag{27}$$

$$F_{\text{ep}} = \sum_{p=1}^{P} \tau_p \cdot 2 \cdot \left(\delta_j - 1.05 \cdot \rho_p\right) \tag{28}$$

$$S_{\text{bc}} = \sum_{t\in\mathcal{T}} p_{\text{out}}(t) \cdot \pi_{\text{sell}}(t) \tag{29}$$

In Equation (26), $\rho_p$ denotes the contracted power for time-of-use period $p$ in kilowatts (kW), $R_p$ is the corresponding power rate in €/kW, and $D_{\text{month}}$ is the number of days in the billing cycle. Equation (27) computes the total cost of energy imported from the grid, where $p_{\text{in}}(t)$ is the energy purchased at time $t$ (in kWh) and $\pi_{\text{buy}}(t)$ is the energy price in €/kWh. Equation (28) calculates penalties for exceeding contracted demand, where $\delta_j$ is the actual measured peak load (kW) and $\boldsymbol{\tau}_p$ is a time-weighting coefficient. Equation (29) accounts for energy sold back to the grid at a fixed export tariff $\pi_{\text{sell}}(t)$, multiplied by the exported energy $p_{\text{out}}(t)$.

### D. Flexible Load Setup

This study models a flexible load corresponding to a 3-kW swimming pool pump operated by the Formentera energy community. The pump is essential for water circulation and filtration and must operate for 8 hours per day. However, its run-time schedule is fully shiftable across the day. A binary decision variable $x_{\text{flex}}(t) \in \{0,1\}$, governs the pump's activation status. When active, it draws its full rated power. The system scheduler can shift the pump operation to periods with greater renewable energy availability or lower grid tariffs, enhancing both self-consumption and economic performance.

TABLE II. Flexible Load Specifications – Swimming Pool Pump

| Parameter | Value | Units | Description |
|---|---|---|---|
| Rated Power | 3 | kW | Constant power draw during operation |
| Daily Requirement | 8 | hours | Must operate 8 hours per day |
| Pump Type | Pool | – | Non-critical, shiftable residential/commercial load |
| Operational Flexibility | Full | – | Schedule adjustable within 24 h window |

Table II summarizes the technical inputs for this flexible load, while Table III presents the scenarios tested to assess the effects of increased flexible load power on system efficiency and NPC. Higher-load cases (4.35 kW and 5.8 kW)

emulate future expansion of load-sensitive equipment like additional pumps.

TABLE III. SCENARIOS FOR FLEXIBLE LOAD DEPLOYMENT

| Flex. Scenario | Pump Power (kW) | Non-flex Load (kWh) | Flexible Energy (kWh) | Daily Runtime (h) | Base Start Time |
|---|---|---|---|---|---|
| 0% | 0 | 211,665 | 0 | 0 | 08:00 |
| 4% | 3 | 202,905 | 8,760 | 8 | 08:00 |
| 6% | 4.35 | 198,963 | 12,702 | 8 | 08:00 |
| 8% | 5.8 | 194,729 | 16,936 | 8 | 08:00 |

## IV. RESULTS AND DISCUSSION

### A. System Sizing and Peak Demand Shaving

Table IV presents system sizing and financial outcomes for each flexibility scenario, comparing the GA–MPC framework with the HOMER Pro baseline. These results are further supported by key performance indicators related to energy flows and asset utilization. As flexibility increases, PV capacity trends slightly downward, from 155 kWp at 0% flexibility to 150 kWp at 8%, yet overall PV generation remains high across all scenarios, exceeding 274 MWh annually. Despite the reduced panel size, improved dispatch and strategic load shifting ensure stable direct PV load coverage, averaging 123 MWh annually. This sustains a consistent PV contribution to total load (~58%), even under varying levels of demand flexibility. Battery storage follows a nuanced path: while HOMER selected 58 strings, the GA–MPC setup installs 76 at 0% flexibility and up to 80 at 8%, matching a steady rise in battery throughput from nearly 83.7 MWh to 85.2 MWh.

TABLE IV. NOVEL METHOD WITH DIFFERENT FLEXIBILITY

| Component | Units | Homer | 0% | 4% | 6% | 8% |
|---|---|---|---|---|---|---|
| Solar PV | kWp | 123 | 155 | 152 | 154 | 150 |
| Battery | Strings | 58 | 76 | 74 | 76 | 80 |
| Inverter | kW | 121 | 77 | 75 | 75 | 72 |
| Contracted Power | kW | 77 | 41 | 40 | 39 | 37 |
| Fuel cell | kW | 5 | 5 | 5 | 5 | 5 |
| Electrolyser | kW | 5 | 6 | 5 | 5 | 5 |
| Tank | Kg | 5 | 7 | 7 | 8 | 9 |
| NPC | € | 661,677 | 612,945 | 606,879 | 604,305 | 599,134 |
| LCOE | €/kWh | 0.241 | 0.224 | 0.221 | 0.221 | 0.218 |

These values indicate intensified battery cycling, critical to shifting solar generation into evening hours, especially as flexibility facilitates midday load realignment, reducing peak stress. Electrolyzer and fuel cell utilization rise markedly compared to the baseline. Electrolyzer capacity factors improve from 10.9% (HOMER) to 30.5% (0% flexibility), while the fuel cell climbs from 2.5% to nearly 10%. This shift results in hydrogen usage growing nearly fourfold, contributing to off-grid autonomy. As flexibility increases, electrolyzer usage slightly declines, but is offset by increased hydrogen storage and battery use, illustrating a balanced reliance between chemical and electrochemical storage. Grid dependency also falls from 15.6% in HOMER to 10% across flexible GA–MPC cases. Grid imports decrease from 33.1 MWh to ~20 MWh, while grid exports double (e.g., from 28.1 MWh in HOMER to 60 MWh in flexible scenarios). This demonstrates the system's enhanced capability to self-supply and even provide net injections during surplus periods, supported by larger storage capacities and dynamic load scheduling.

Economically, the system demonstrates cost-performance benefits as flexibility increases. The NPC drops from €661,677 (HOMER) to €599,134 (MPC 8%), while the levelized cost of electricity (LCOE) improves from €0.241/kWh to €0.218/kWh. These improvements stem from more efficient asset usage and lower reliance on the grid. Notably, annual grid imports fall by over 38%, from 33.1 MWh (HOMER) to 20.5 MWh ( 8%), which directly cuts grid purchase costs. In parallel, surplus generation increases, with annual exports nearly doubling to over 60 MWh in flexible scenarios, enabling additional revenue streams. This shift in energy flow also reduces grid-related operational expenditures from €29,525 (HOMER) to €15,886 (8%), a reduction of 46.2%. These savings, combined with flatter investment profiles, illustrate how modest demand-side flexibility can significantly enhance project-level economic viability. In essence, the rolling-horizon framework not only reduces oversizing but also enhances asset utilization and project economics by integrating modest demand flexibility with daily re-optimisation.

### B. Load Shifting and Daily Operational Behaviour

Fig. 1 illustrates three consecutive high-irradiance days in August under the GA–MPC 8% scenario. The controller strategically shifts the 5.8 kW flexible load toward evening hours (16:00–23:00), where it better aligns with remaining battery capacity and avoids midday price peaks. Across the three days, midday PV generation exceeds 570 kWh/day, allowing substantial battery charging (~200 kWh) and surplus grid exports (~200 kWh/day). Morning and night loads are predominantly met by batteries, ensuring grid independence during high-tariff periods. Compared to HOMER's load-following strategy, which lacks demand flexibility and requires early-morning grid imports (>100 kWh) despite the same high-irradiance summer days, MPC achieves lower grid usage, greater energy autonomy, and enhanced economic performance through demand reshaping and energy sales.

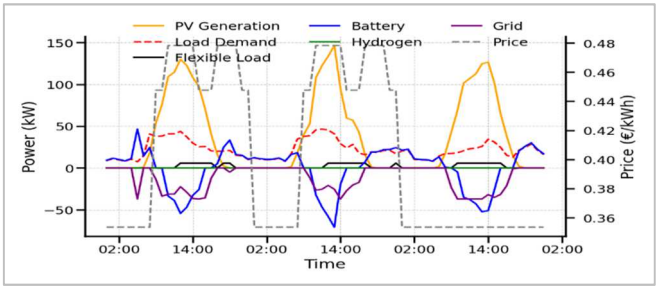


Fig. 1. GA–MPC summer profile showing load shifting.

In contrast to the summer surplus dynamics, winter days exhibit low PV output and thus demand tighter coordination of storage and grid usage. Operational profiles for three January days under the 8% scenario showcase its ability to adaptively schedule flexible loads to minimize grid imports during peak-tariff windows. On weekdays, 8% flexibility allows shifting water pump operation to low-tariff early morning hours (00:00–07:00) and evening periods (16:00–23:00), avoiding costly daytime rates. Midday PV (~220–530 kWh) is allocated efficiently across battery charging, hydrogen production, and direct load supply. Despite flat

tariffs on weekends, MPC still optimizes by aligning pump operation with solar peaks, preserving battery reserves. Compared to HOMER's load-following strategy, characterized by reactive dispatch, low SOC%, and heavier grid reliance, the GA–MPC controller demonstrates higher autonomy, limited high-price grid exposure, and greater renewable exploitation, even under constrained winter conditions.

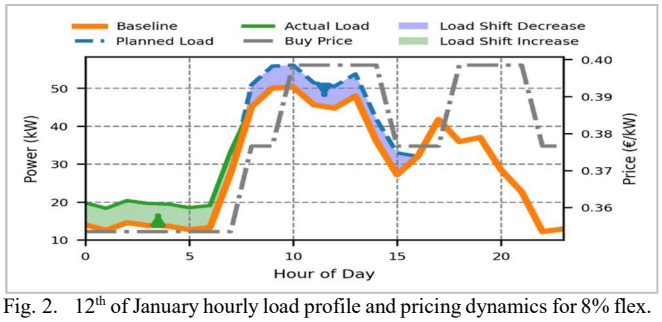


Fig. 2. 12th of January hourly load profile and pricing dynamics for 8% flex.

As an illustrative winter case, Fig. 2 shows the MPC-8% operational profile for 12 January. With limited PV availability and variable electricity prices (€0.3535–€0.4782/kWh), the controller shifts most of the flexible load to the early morning (00:00–07:00), fully exploiting the lower tariff window. Battery discharge supports demand during this period, preserving grid independence. As PV ramps up midday (~11:00–15:00), generation is prioritized for charging (~100 kWh) and hydrogen production, while surplus is exported during peak-price hours, minimizing imports. Compared to benchmark strategies, this targeted scheduling avoids high daytime tariffs and better aligns with solar output, exemplifying the GA–MPC framework's adaptive logic under constrained winter conditions.

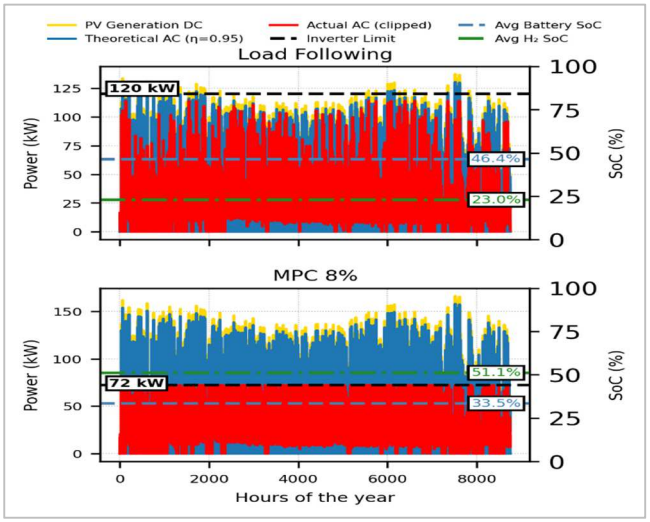


Fig. 3. Inverter use and average SoC under HOMER and 8% solution.

This relationship between sizing decisions and operational dynamics is further illustrated in Fig. 3, which compares inverter utilization and storage behaviour across the year. While HOMER employs a larger 120 kW inverter, the MPC 8% solution achieves similar annual AC output using a smaller 72 kW inverter, enabled by a larger PV array, expanded storage, and coordinated control. The higher average hydrogen SoC (51.1%) versus battery SoC (33.5%) reflects the MPC strategy's temporal separation of roles: batteries handle daily balancing, while hydrogen smooths seasonal mismatches. This enables higher renewable penetration and efficient inverter use without excess clipping.

## V. CONCLUSION

This study introduced a bi-level GA–MPC optimisation framework that dynamically co-optimizes capacity sizing and dispatch operations in hybrid renewable energy systems, with specific application to islanded contexts like Formentera. By explicitly treating inverter sizing, grid subscription, and load flexibility as decision variables, the framework achieves substantial reductions in grid dependency, system costs, and operational emissions. The 8% flexible-load scenario reduced Net Present Cost by 9.4%, grid import by 38%, and operational expenditure by 46% compared to the HOMER baseline. Despite a smaller inverter and higher PV capacity, the GA–MPC system achieved higher renewable penetration, leveraging dynamic load shifting and seasonal storage via hydrogen. Hourly simulations reveal enhanced self-consumption, export revenue, and system autonomy under varying seasonal and pricing conditions. These findings underscore the importance of integrated design and control strategies in achieving cost-effective and resilient energy systems for islands and other constrained grids.

## VI. REFERENCES


[1] Directorate-General for Energy, "In focus: EU islands and the clean energy transition," Brussels, Jul. 15, 2021. Accessed: Jun. 21, 2023. [Online]. Available: https://commission.europa.eu/news/focus-eu-islands-and-clean-energy-transition-2021-07-15_en

[2] Eurostat, "Tourism peak months differ across EU regions." Accessed: Sep. 04, 2024. [Online]. Available: https://ec.europa.eu/eurostat/web/products-eurostat-news/w/ddn-20231130-2

[3] M. F. Roslan, M. A. Hannan, P. J. Ker, and M. N. Uddin, "Microgrid control methods toward achieving sustainable energy management," *Appl. Energy*, vol. 240, pp. 583–607, Apr. 2019, doi: 10.1016/j.apenergy.2019.02.070.

[4] A. I. Atteya and D. Ali, "Benchmarking a Novel Particle Swarm Optimization Dynamic Model Versus HOMER in Optimally Sizing Grid-Integrated Hybrid PV–Hydrogen Energy Systems," *Eng*, vol. 5, no. 4, Art. no. 4, Dec. 2024, doi: 10.3390/eng5040170.

[5] F. Firdouse and M. Surender Reddy, "A hybrid energy storage system using GA and PSO for an islanded microgrid applications," *Energy Storage*, vol. 5, no. 7, p. e460, 2023, doi: 10.1002/est2.460.

[6] P. Marocco, D. Ferrero, E. Martelli, M. Santarelli, and A. Lanzini, "An MILP approach for the optimal design of renewable battery-hydrogen energy systems for off-grid insular communities," *Energy Convers. Manag.*, vol. 245, p. 114564, Oct. 2021, doi: 10.1016/j.enconman.2021.114564.

[7] N. Niveditha and M. M. Rajan Singaravel, "Optimal sizing of hybrid PV–Wind–Battery storage system for Net Zero Energy Buildings to reduce grid burden," *Appl. Energy*, vol. 324, p. 119713, Oct. 2022, doi: 10.1016/j.apenergy.2022.119713.

[8] K. Tamashiro, E. Omine, N. Krishnan, A. Mikhaylov, A. M. Hemeida, and T. Senjyu, "Optimal components capacity based multi-objective optimization and optimal scheduling based MPC-optimization algorithm in smart apartment buildings," *Energy Build.*, vol. 278, p. 112616, Jan. 2023, doi: 10.1016/j.enbuild.2022.112616.

[9] F. A. Kassab, B. Celik, F. Locment, M. Sechilariu, S. Liaquat, and T. M. Hansen, "Optimal sizing and energy management of a microgrid: A joint MILP approach for minimization of energy cost and carbon emission," *Renew. Energy*, vol. 224, p. 120186, Apr. 2024, doi: 10.1016/j.renene.2024.120186.

[10] VPP4ISLANDS Consortium, "Virtual Power Plant for Interoperable and Smart isLANDS," VPP4ISLANDS. Accessed: Jun. 14, 2023. [Online]. Available: https://vpp4islands.eu/

[11] National Aeronautics and Space Administration (NASA) Langley Research Center, "POWER Data Access Viewer," NASA POWER. Accessed: Aug. 06, 2024. [Online]. Available: https://power.larc.nasa.gov/data-access-viewer/